

Spectral analysis of water vapour in cool stars

Hugh R. A. Jones¹, Yakiv Pavlenko², Serena Viti³, Jonathan Tennyson³

¹*Astrophysics Research Institute, Liverpool John Moores University, Egerton Wharf, Birkenhead CH41 1LD, UK*

²*Main Astronomical Observatory of Ukrainian Academy of Sciences, Golosiiv woods, 03680 Kyiv-127, Ukraine*

³*Department of Physics and Astronomy, University College London, Gower Street, London WC1E 6BT, UK*

Accepted Received

ABSTRACT

M star spectra, at wavelengths beyond 1.35 μm , are dominated by water vapour yet terrestrial water vapour makes it notoriously difficult to make accurate measurement from ground-based observations. We have used the short wavelength spectrometer on the Infrared Space Observatory at four wavelength settings to cover the 2.5–3.0 μm region for a range of M stars. The observations show a good match with previous ground-based observations and with synthetic spectra based on the Partridge & Schwenke (1997) line list though not with the SCAN (Jorgensen et al. 2001) line list. We used a least-squared minimisation technique to systematically find best fit parameters for the sample of stars. The temperatures that we find indicate a relatively hot temperature scale for M dwarfs. We consider that this could be a consequence of problems with the Partridge & Schwenke linelist which leads to synthetic spectra predicting water bands which are too strong for a given temperature. Such problems need to be solved in the next generation of water vapour line lists which will extend the calculation of water vapour to higher energy levels with the good convergence necessary for reliable modelling of hot water vapour. Then water bands can assume their natural role as the primary tool for the spectroscopic analysis of M stars.

Key words: stars: low-mass, brown dwarfs; stars: late-type; stars: abundances; stars: fundamental parameters; stars: atmospheres

1 INTRODUCTION

More than two-thirds of stars within 10 parsecs are M dwarfs and it is very probable that this number density prevails throughout our Galaxy. Unless there is a sharp turn-down in the stellar mass function, they and even lower mass objects are a major component of the Galaxy's mass. The dominant red and infrared luminosity of the underlying stellar population of galaxies is from M giants. The dominant source of opacity for late-type M dwarfs, giants and brown dwarfs is water vapour which easily forms in their relatively high pressure, low temperature atmospheres. Leaps in theoretical molecular quantum mechanics and computer hardware capabilities mean that it is possible to perform ab initio calculations to accurately predict the frequency and intensity for ro-vibrational transitions for water vapour. This means that it is no longer necessary to extrapolate laboratory measurements for water vapour to untestable temperature regimes of which are found in the atmospheres of M dwarfs.

The preponderance of water vapour in the Earth's atmosphere makes it very difficult to observe its spectral signature in stars. At near-infrared wavelengths, where cool stars emit most of their flux, the strongest water vapour

absorption band is centred around 2.65 microns where the atmosphere is opaque (Fig. 1). The advent of the Infrared Space Observatory has for the first time allowed observations to be made at the peak of water vapour absorption in cool stars. Such data are not only impossible to obtain from terrestrial sites but also provides a vital overlap with ground-based data. For M dwarfs this is essential as the data reduction problems of decontamination of stellar and terrestrial water vapour are never far away.

2 OBSERVATIONS

The spectral region required for this program is inaccessible from ground-based observatories and is well matched to ISO capabilities. SWS and ISO provide sufficient resolution to resolve individual ro-vibrational water bands with enough sensitivity to observe the intrinsically faint and cool M dwarfs. The strategy was to observe a sample of M dwarfs which are bright enough to obtain high signal-to-noise spectra. The ISO programme for these observations is known as JONES_PROP32.

We observed a range of M dwarfs - GJ 752B (M8V),

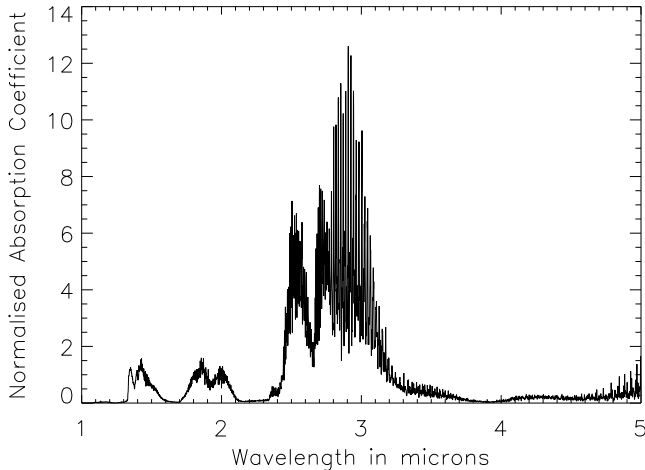


Figure 1. The water vapour absorption coefficient at 3000 K across the peak of the flux distribution for late-type M and brown dwarfs. The plot has been normalised to one around the maximum absorption of water vapour that can reliably be observed from the ground (‘high opacity’ case in Jones et al. 1994).

Table 1. Properties and total integration times for the sample.

Object	Flux, Jy ($2.76\mu\text{m}$)	Spectral Type	Time, s
GJ 191	4.13 ± 0.09	M2.5VI	4530
GJ 699	6.66 ± 0.14	M4V	1192
GJ 406	1.503 ± 0.031	M6V	9839
GJ 752B	0.019 ± 0.020	M8V	18216
BS 8621	509.7 ± 4.1	M4III	1238

GJ 406 (M6V), GJ 699 (M3.5V) and GJ 191 (M2VI) together with the M4 giant BS 8621. The M dwarfs were chosen because they have been the subject of previous studies of M dwarfs (e.g. Jones et al. 1996). The observations were made in with the Short Wavelength Spectrometer (SWS) in its full resolution grating mode known as SWS06. Observations were made using bands 1A and 1B covering the wavelength ranges 2.48–2.60, 2.60–2.75, 2.74–2.90 and 2.88–3.02 μm . These grating scans also gave simultaneous coverage from 15.99–16.25 and 16.03–16.21 μm , however, the relatively low flux levels of the M dwarfs (< 10 Jy) and the lower sensitivity of the instrument means that no useful data were recorded.

3 DATA REDUCTION

The observational data were processed within the Observers SWS Interactive Analysis Package from the standard processed data to Auto Analysis Result level through the standard pipeline of Derive Auto Analysis Product. In addition to a few bad data points flagged by the auto analysis software ISO, SWS data also contains glitches and jumps not easily corrected for by the standard reduction tools (Heras 1997). The philosophy adopted for the data presented here was to ignore all scans effected by glitches or jumps and to let individual bad points be taken care of by sigma clipping. The glitches and jumps do not tend to appear in the brighter objects though for the fainter objects, e.g., GJ 406,

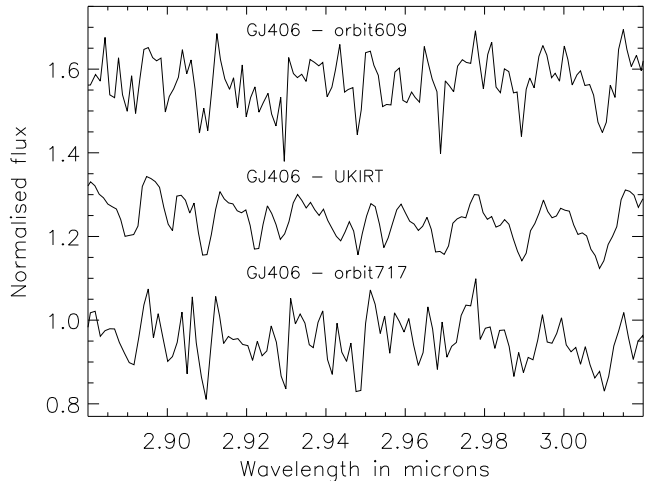


Figure 2. A comparison of datasets for GJ 406 from orbits 609 and 717 of this programme and from UKIRT data from Jones et al. (1995). This object has the lowest signal-to-noise ratio in our analysis yet shows a reasonable agreement between spectra taken on different orbits and from the ground.

they affect around 10 percent of scans. The `proc_band` and `div` procedures were used to print out scans for each individual detector for each observation for all targets. These were visually inspected to check for glitches, and bad data points. The ISO Spectral Analysis Package (ISAP) was used to remove bad data points, check the data and to produce the final combined spectra by averaging across all detectors using the standard clip mean option. We found little sensitivity to the method used to combine the data.

We also made observations of the archetypal late-type M dwarf GJ 752B. These data are tantalising however our conservative reduction philosophy means that little of this data survives. It would be possible to flag all glitches and jumps, however, they are usually accompanied by gradients affecting most of the data in a scan. We look forward to the advent of reduction tools that will be able to deal with flux levels at the 0.01 Jy level.

The calibration files used for the reduction were those included in version 8.4 of ISAP package. Based on comparisons between objects taken with the same configuration during different orbits the flux calibration varies by only a few percent. This is expected for band 1 SWS observations which have excellent calibration. The wavelength calibration for the SWS instrument is measured to be within 1/8 of a resolution element (Salama et al. 2000). The available ground-based data for our sample are at lower resolution than the ISO data, nonetheless, bear out the calibration of the SWS data. Fig. 2 shows the good agreement in the region of overlap between parts of the dataset taken on different orbits and ground-based measurements (from Jones et al. 1995).

4 AVAILABLE WATER LINELISTS

The crucial opacity for M stars across the range of our observed spectra is water vapour (e.g., Fig. 5). A useful

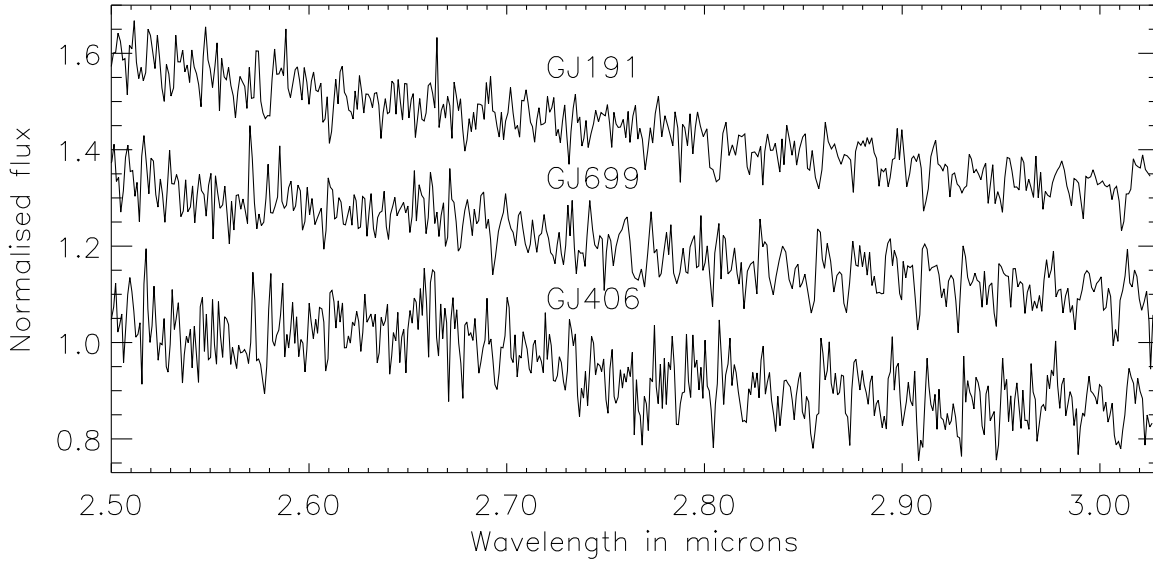


Figure 3. A spectral sequence for GJ 191 (M2VI), GJ 699 (M4V) and GJ 406 (M6V).

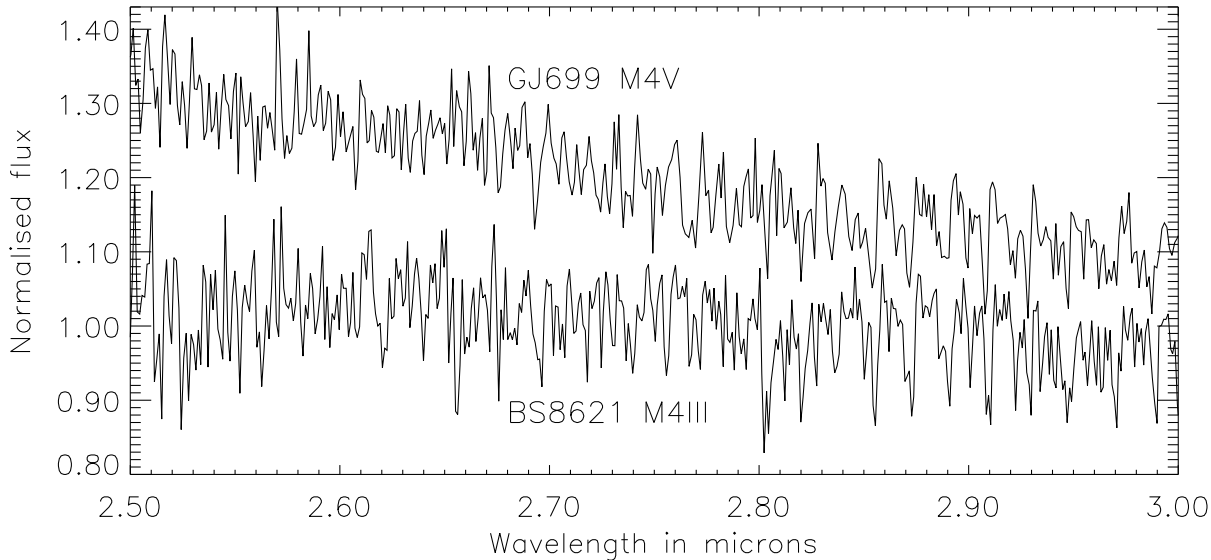


Figure 4. A comparison at optical spectral type M4 for the dwarf (V) GJ 699 and the giant (III) BS 8621.

model atmosphere thus needs to include an appropriate water linelist. There are several different sources of water data and a few of them have been investigated here. A reliable water linelist needs: 1. a good (electronic) potential energy surface; 2. well converged nuclear motions (i.e vibration-rotation) calculations; 3. a reliable dipole surface. To date, it is not yet possible to get a completely reliable *ab initio* potential surface, so all the linelists discussed in this paper used surfaces which have been adjusted to reproduce laboratory spectroscopic data for water. Fitting to lab data can cause problems in regimes where such data are unavailable (Polyansky et al. 1997a). Conversely tests (Lynas-Gray, Miller & Tennyson 1995) have shown that *ab initio* dipole

surfaces are much more reliable than the ones fitted to experimental data.

The water vapour data investigated in this paper are from Miller et al. (1995, known as the MT list), from Partridge & Schwenke (1997, known as the PS or AMES list), from Jorgensen et al. 2001 (known as SCAN), and from Viti (1997, known as the VT2 linelist) which superseded the MT and VTP1 line lists (Viti, Tennyson & Polyansky 1997). MT is a relatively small list (10 million lines) which used, by today's standards, a rather inaccurate potential. VTP1 energy surface is much more accurate than MT but it is still not complete enough for stellar models. VT2 is a much larger linelist (> 300 million lines) which uses a potential surface reliable for higher vibrational states. However, due to seri-

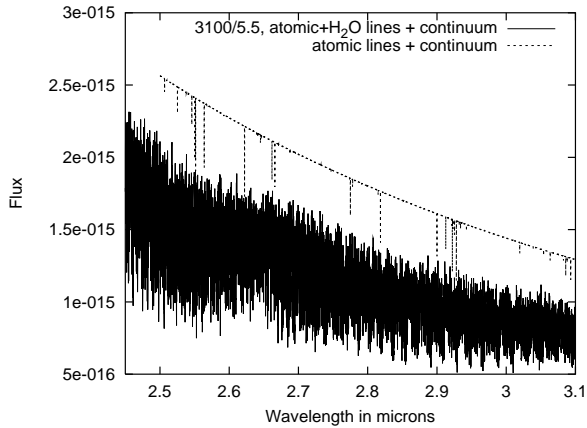


Figure 5. Theoretical SEDs computed for 3100/5.5 model atmosphere taking into account continuum + atomic line and continuum + atomic lines + H₂O opacities

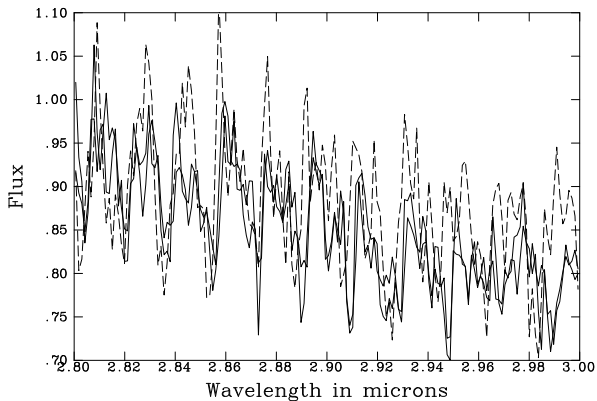


Figure 6. GJ 406 compared with 3000 K synthetic spectra using the MT and PS line lists. The observed spectra and PS model are shown as solid thick and thin lines respectively and the MT model as a dotted line. The match of water bands between observations and model is considerably better for the PS model.

ous computer format corruption problems this list could not be included in model atmospheres calculations.

5 SPECTRAL ANALYSIS

For this analysis we computed spectral energy distributions for a range of model atmosphere parameters: effective temperatures, $T_{\text{eff}} = 2700 - 3900$ K, metallicities $[\text{Fe}/\text{H}] = 0.0 - -1.5$ and gravities $\log g = 0.0 - 5.5$. From here on we refer to these as model synthetic spectra. These were generated using the temperature structures from the model atmospheres of Hauschildt, Allard & Baron (1999) by the WITA6 program (Pavlenko 2000). In our computations we used the atomic line list from VALD (Kupka 1999), the water vapour line lists of Partridge & Schwenke (1998) and Jorgensen (2001) and the CO line list of Goorvitch (1994).

We also used synthetic spectra from the PHOENIX

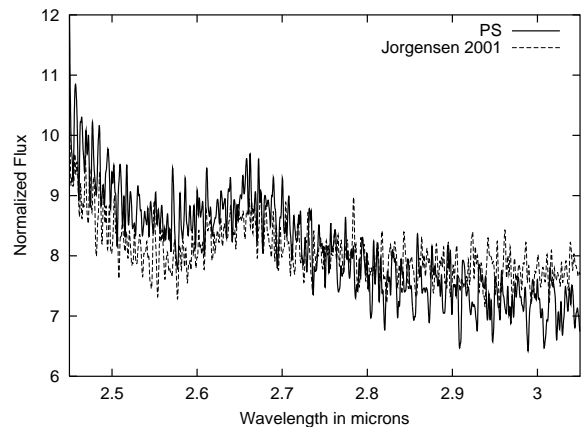


Figure 7. Comparison between synthetic spectra at 3100 K using the SCAN and PS line lists.

model atmosphere code, the so called NextGen version 5 (Hauschildt et al. 1999).

We adopt the Voigt function $H(a, v)$ for the line shape of any line in our computations. Damping constants $a = (\gamma_2 + \gamma_4 + \gamma_6)/(4 \times \pi \times \Delta\nu_D)$ are determined in atmospheres of cool dwarfs mainly by Van der Waals (pressure) broadening ($n=6$) and (in upper layers) natural broadening ($n=2$). Stark broadening ($n=4$) of spectral lines can be neglected here due to low temperatures and electron densities. For atomic lines the line broadening constants were taken from VALD. Unfortunately, for molecular line broadening models are rather uncertain. We assume that the mechanisms of broadening molecular and atomic lines are similar. Radiative broadening of molecular lines were computed in the frame of classical approach $\gamma_2 = 0.22/\lambda^2$ (Allen 1973). Due to the high pressures and low temperatures in the atmospheres of cool dwarfs Van der Waals broadening should dominate there (see Pavlenko 2001). The damping constants of pressure broadening of molecular lines γ_6 were computed following Unsold (1948).

To provide an idea of the improvement since our previous work (Jones et al. 1995), in Fig. 6 we compare GJ 406 with 3000 K synthetic spectra generated using the PS and MT lists. As with Jones et al. (1995) we found that the intensities of the water band strengths seem to be reasonably well

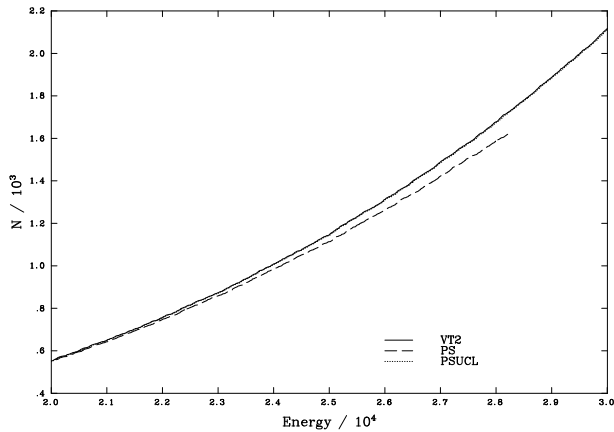


Figure 8. Number of energy levels as a function of energy for PS (dotted) and VT2 (continuous) linelist for $J = 17$. The PS linelist stops at 28000 cm^{-1} .

determined. However, we find that the PS line list prediction of bands with wavelength is a substantial improvement on the previously used MT line list. We also investigated using the SCAN line list (Jorgensen et al. 2001) and in Fig. 7 compare this to the PS list. As with our previous comparisons to the SCAN list (Jones et al. 1996) we find the predicted shape of the water bands as well as the structure of the bands are rather different from other models and observations. As expected from the scale of the calculation and previous comparisons with observations (e.g., Allard et al. 2000) we find that the PS line list is the most useful water line list available for our observed data. We first proceed to investigate the completeness of the PS line list and then use it to find best-fit parameters for our targets.

5.1 Completeness of the PS line list?

For model atmospheres with effective temperatures in the range $2000 - 4000 \text{ K}$, Boltzmann considerations suggest that transitions involving states with $J = 20 - 30$ are the dominant sources of opacity. We find two problems with the PS linelist: (i) first of all, it does not reach 30000 cm^{-1} for any J apart from $J = 0$. On average it gets to 28000 cm^{-1} . (ii) Secondly, even by truncating energy levels to 28000 cm^{-1} , VT2 still has more levels than PS has for high J , for example, at $J = 17$, VT2 gives 100 energy levels more than PS below 28000 cm^{-1} . From the number of energy levels missing for each J we estimate that PS omits $\sim 30\%$ transitions up to $J = 10$; $\sim 50\%$ up to $J = 20$; and $\sim 60\%$ up to $J = 28$.

As a test, a new set of energy levels using the PS potential energy surface, the same atomic masses as PS and VT2 nuclear motion parameters, were computed. This new set of energy levels is known as UCLPS (University College London Partridge Schwenke list; see Polyansky et al. 1997b for further comparisons). This was done to test the variational convergence for the same potential energy surface. An example of the energy levels comparison with VT2 and the new calculations is shown for $J = 17$ in Fig. 8. The calculations performed with the PS potential energy surface are in close agreement with VT2 which suggests that the lack of

states in the PS linelist is due to poor convergence and not to differences in the potential energy surface used. In fact, close examination of the parameters of the PS calculation strongly suggests that their decision not to increase the size of the Hamiltonian matrix beyond that used for $J = 4$ resulted in poorly converged calculations for higher states with high J . This decision undoubtedly saved them from some of the computational problems experienced in the computation of the VT2 linelist (Viti 1997).

For low- J energy levels, PS's calculations give superb results, reproducing experiment with a much higher accuracy than VTP1 or VT2. However, for higher rotational states, particularly those with $J > 20$, we find that a very high proportion of rotational states which one expects to be degenerate in fact show significant splittings in the PS linelist. This splitting is not shown in VTP1, VT2 or in UCLPS. In particular for the levels with high K_a and with K_c odd (where K_a and K_c are the projections of J on the A and C principal axes of rotation of asymmetric top molecules), all lie below the ones with K_c even for levels with which they should be quasi-degenerate. Since the PS calculation truncates variational rotation-vibration calculations with 7500 energy-selected basis functions independent of the rotational parity this means that the K_c odd calculations will contain states of higher cut-off energy than the K_c even calculation. The variational principle means that the K_c odd states will be better converged and hence lower in energy.

This causes two problems. Firstly, artificial splitting of lines means that it is difficult to use the list for line assignments (Polyansky et al. 1997a). The second is more subtle. An important consideration in radiative transport is how the line absorptions fill in gaps in the spectrum. Two transitions which, to within their linewidth, are coincident will have less effect on the opacity than two separate transitions. Artificially doubling the number of lines for these J values is likely to cause the strength of water vapour bands at low resolution to be overestimated.

It should be noted that the resolution of the observed spectra (see Fig. 2) is much too low to see the rotational structure of H_2O shown in the theoretical spectrum (Fig. 5). Although the calculated line positions of the PS list agree well enough with the experimental ones (tabulated, for example, in HITRAN96, Rothman et al. 1996), individual line strengths can differ greatly. Recently Schwenke & Partridge (2000) found problems with their analytical representation of the *ab initio* dipole moment data used for the computation of the PS linelist: this may have led to an overestimation of the intensities of weak bands with respect to experimental data. They improve their previous analytical representation by careful and accurate fitting. However their new dipole surface has yet to be used to produce an improved water linelist.

5.2 Best-fit parameters

Our synthetic spectrum models were calculated at high resolution, typically $0.5 - 1 \text{ \AA}$. Before comparison with model spectra were made the observed data were corrected for their radial velocities: 244.0 , 110.9 and 21.0 km/s respectively for GJ 191, GJ 699 and GJ 406 (Leggett 1992). The model were transformed to the resolution of the data and to wavelengths

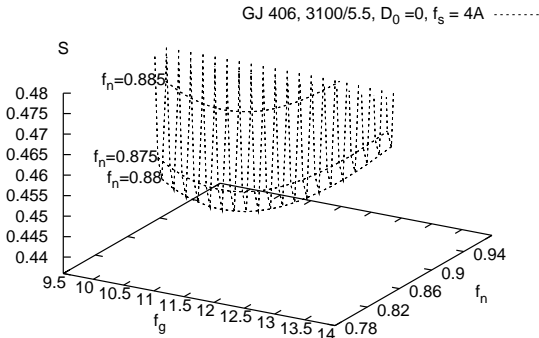


Figure 9. An example of the dependence of S on f_n and f_g , values of f_n and f_g are in Å.

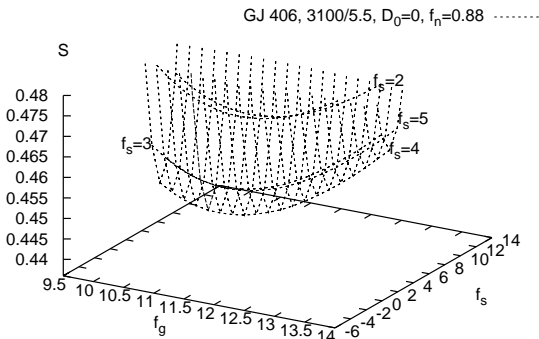


Figure 10. An example of the dependence of S on f_s and f_g , values of f_s and f_g are in Å.

in air. The resolution of ISO data are actually somewhat uncertain and have been the subject of a number of studies (e.g. Valentijn et al. 1996, van den Ancker et al. 1997, Lutz, Feuchtgruber & Morfill, 2000). The SWS06 mode is a grating scan mode and in principle reproduces the full intrinsic resolution of the grating (so-called SWS02 mode). However, the SWS06 mode has poor sampling of a given wavelength element. For the purpose of the derivation of high-fidelity line profiles, this causes unwanted interactions between line profiles and the relative sensitivities for the 12 detectors of a band ('flat-fielding in SWS-speak'), since all twelve detectors have to be combined for a good profile. This means that although the measured resolution of SWS02 in band 1A (2.38 — 2.60 μm is 0.0007 μm and 0.0011 μm in band 1B (Lutz et al. 2000), the actual resolution of these SWS06 spectra is likely to be somewhat less.

In order to determine the best fit parameters for our targets in a systematic fashion, we performed a least-squared minimisation on the spectra within a grid of synthetic spectra using the PS line list. As with the previous work we noticed that the form of the observed spectra along with its unresolved nature means that the line broadening employed by the models has a substantial influence on the fits. Although the SWS line profile is well determined to within 1

per cent, the resolution of the data are not so secure (Lutz et al. 2000). To find the best fit model parameters we allowed the spectral normalisation, wavelength shift and resolution to vary.

We compared observed fluxes H_λ^{obs} with computed values $f_n * H_{\lambda+f_s}^{\text{theor}}$. We let $H_{\text{lambd}}^{\text{obs}} = \int (F_{x-y}^{\text{theor}} * G(y)) * dy$, where the theoretical flux is F_λ^{theor} and $G(y)$ is the instrumental profile modelled by a Gaussian. In our case $G(y)$ may be wavelength dependent. To get the best fit we find the minima per point of the 3D function

$$S(f_n, f_s, f_g) = \Sigma(1 - H^{\text{synt}}/H^{\text{obs}})^2.$$

We calculated this minimisation with each observed spectrum and the grid of synthetic spectra, to determine a set of parameters f_n (normalisation factor), f_s (wavelength shift parameter), f_g (resolution) for all the stars of our sample.

In general we found the dependence of S on f_n and f_s is much stronger than on the f_g . For example see Fig. 9 and 10 for the case GJ 406. It should be noted that although the resolution across a grating setting is expected to be the same the resolution is expected to decrease slightly between the so called band 1A (2.48 — 2.60 μm) and band 1B (2.60 — 3.02 μm) data. We account for this by also investigating the band 1A and band 1B data separately. Best fit values for f_g were investigated for the observed spectra, across most of the grid of model atmospheres. They ranged from 7.0 (band 1A) to 18.2 (band 1B) Å and always showed the expected resolution difference between band 1A and 1B data, e.g., example minimisation plots are shown for GJ 406 and a 3100 K, $\log g = 5.5$, solar metallicity model in Figs 9 and 10. We generally found the largest and smallest values for f_g when making comparisons with synthetic spectra with properties far from the best fit minimisation S values. For example in the case of GJ 406, the extreme best fit f_g values of 8.0 and 18.2 Å are obtained with synthetic spectrum models of 3300 K, $[\text{Fe}/\text{H}] = -1.5$ and 2700 K, $[\text{Fe}/\text{H}] = 0.0$ respectively. Apart from giving us an independent check of the resolution, this procedure served to investigate the sensitivity of minimisation S values to resolution f_g . Although different f_g 's give significantly different values of S we found that the best fit temperature for a given f_g was stable. We also found S values for *observed* and synthetic spectra smoothed by the same effective values. Although this gave the same best fit minimisation synthetic spectra, this conservative solution involves smoothing the observed data and led to a decrease in the sensitivity of the best fit solution. Given the numerical stability of our best fits to resolution and the lack of evidence for any changes in the SWS resolution with time we felt confident using the adopting the resolution values of 0.0012 and 0.0017 μm for band 1A and band 1B data as given in the SWS Observer's manual (de Graauw et al. 1996).

Our minimisation procedure also yields normalisation values f_n for the different spectral regions. We find that the band 1A data are fainter than the band 1B data by 1–2% using our best fit synthetic spectra. Given that this is generally better than the formal signal-to-noise of our spectra and that this result is somewhat model dependent we thus consider the flux calibration of the data to be robust and do not apply any new flux calibration to the data. The minimisation procedure also yields values for the wavelength shift f_s . We found a shifts of 3.7–4.3 Å between observed

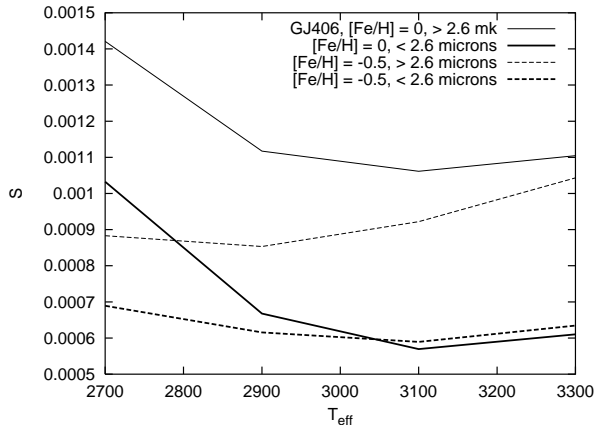


Figure 11. Minimisation S for different synthetic spectra compared to GJ 406 spectrum.

and synthetic spectra which corresponds to around 0.3 of our data resolution. This shift maybe due to the wavelength calibration of the data though at least part may arise from inaccuracies in the water vapour line list used to generate the synthetic spectra.

Our results are also sensitive to the rather uncertain damping parameters adopted for molecular lines. To test this dependence two models at 2700 K, $\log g = 5.5$, $[\text{Fe}/\text{H}] = -0.5$ with different damping constants were compared. The literature for atomic lines (e.g., Gurtovenko & Kostyk 1989) tells us that that a factor of two might be the maximum expected for this uncertainty due to the difference between classical and quantum mechanical computations. Although both atomic and molecular lines are damped oscillations the oscillations are greater in molecules so a larger factor maybe appropriate. Nonetheless it is also possible that molecular lines are less sensitive to damping because the structure of molecular levels maybe more flexible to changes of the surrounding electric fields: electrons of molecular orbitals are less bound in comparison with atoms. There may be something like a “soft (quasi-)adiabatic response”. We conducted a rather conservative experiment and compared models using Unsold’s γ_6 and with $5 \times \gamma_6$ and found a flux difference of around 5%. For our comparisons we consider this is an upper limit as in all cases we are investigating weaker molecular bands, due to higher effective temperatures and/or lower metallicities. Furthermore, we are investigating the spectral differences in terms of synthetic spectra at relatively low resolution and find the expected uncertainty due to molecular damping constants to be much less than 1% and so not significant for our results.

The following subsections investigate our fits to the each observed spectra in turn. The best fit models are then compared with a compilation of values from the literature in Section 5.6.

5.3 GJ 406

As discussed above and as illustrated in Figs 9 and 10 we carried a number of different tests on GJ 406 in order to find our preferred model fits. We tended to use GJ 406 as our primary observed spectrum because of its late spectral type and strong water bands. In addition to the tests dis-

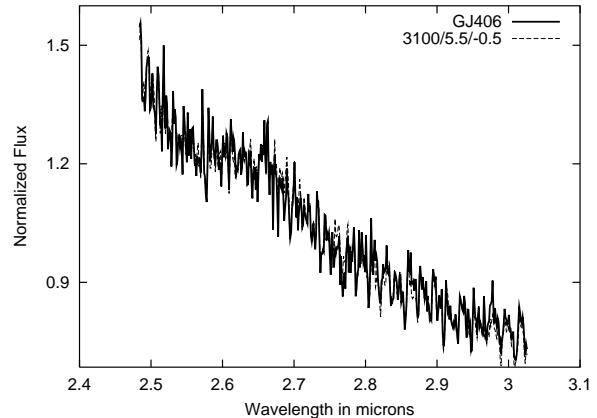


Figure 12. The observed spectrum of GJ 406 compared to a 3000 K, $\log g = 5.5$, $[\text{Fe}/\text{H}] = -0.5$ synthetic spectrum.

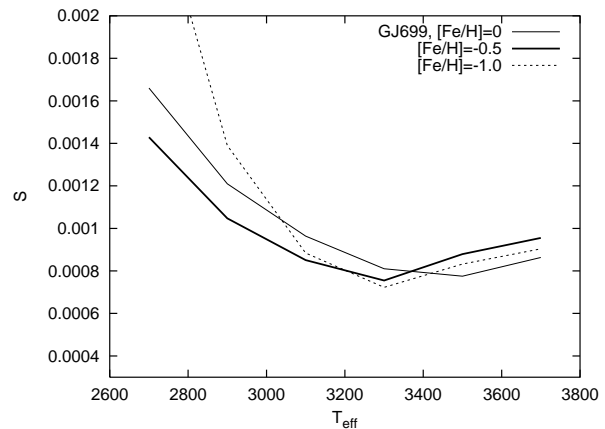


Figure 13. Minimisation S for different synthetic spectra compared to GJ 699 spectrum.

cussed above GJ 406 has data taken during four different orbits which allows us to analyse the orbits separately, thus checking any time dependence problems with the dataset. We found differences in the minimisation values obtained of around 7% for the 2.48–2.90 μm data and around 20% for the 2.88–3.02 μm data though the best fit models were all within 100 K.

Fig. 11 illustrates the minimisation, S for various different synthetic spectra with the observed GJ 406 spectrum. For this plot we have split up the fits into those for data shortward and longward of 2.6 μm . The improved minimisation for the higher resolution $< 2.6 \mu\text{m}$ data can be seen. As can the rather complex sensitivity of the minimisation with temperature and metallicity. The best fit value appears to be for $[\text{Fe}/\text{H}] = -0.5$ and 3000 K with the solar metallicity models suggesting 3100 K and $[\text{Fe}/\text{H}] = -1.0$ models suggesting 2900 K. An illustration of the quality of the fit can be seen in Fig. 12

5.4 GJ 699

GJ 699 (Barnard’s star) is the largest proper motion object known outside our solar system and is thus suspected of being relatively old and having a low metallicity. In fact it

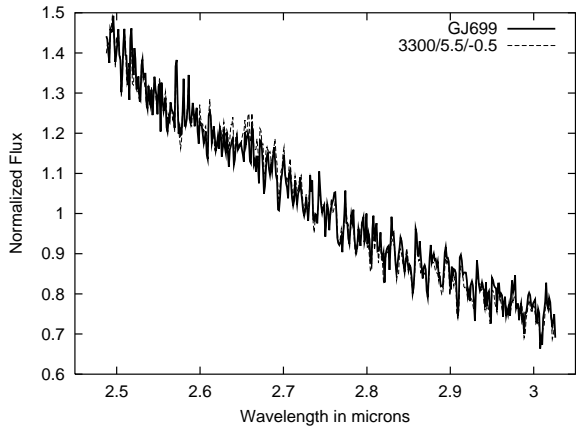


Figure 14. The observed spectrum of GJ 699 compared to a 3300 K, $\log g = 5.5$, $[\text{Fe}/\text{H}] = -0.5$ synthetic spectrum.

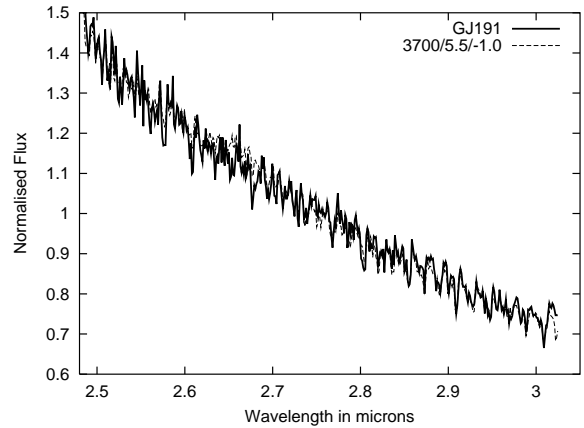


Figure 16. The observed spectrum of GJ 191 compared to a 3700 K, $\log g = 5.5$, $[\text{Fe}/\text{H}] = -1.0$ synthetic spectrum.

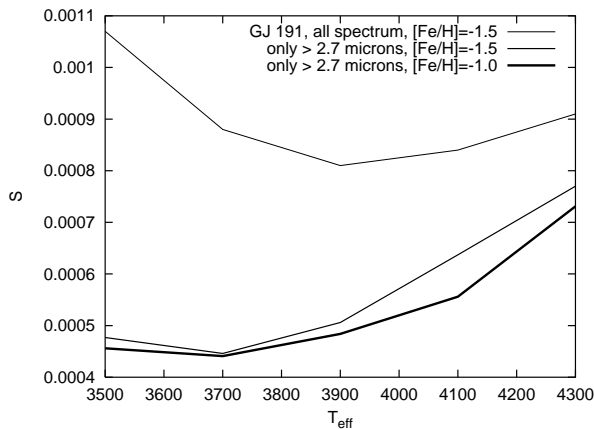


Figure 15. Minimisation S for different synthetic spectra compared to GJ 191 spectrum.

tends to skew the proper motion properties and characteristics of the local neighbourhood so much that it is sometimes ignored from such studies. Nonetheless it is the most nearby and brightest known M4V dwarf and thus was included as target for this programme. Fig. 13 shows the minimisation plot for the observed spectrum. This suggests a best fit synthetic spectrum with 3300 K and $[\text{Fe}/\text{H}] = -0.5$. In Fig. 14 we compare this fit with the observed spectrum.

5.5 GJ 191

GJ 191 has a high space velocity and displays CaH bands in its optical spectra and unlike GJ 699 is indisputably spectrally typed as a subdwarf. Our analysis of $S = f([\text{Fe}/\text{H}], T_{\text{eff}})$, e.g., Fig. 15, showed a best fit temperature of 3700 K and $[\text{Fe}/\text{H}]$ values in the range -1.0 — -1.5 . Computations with larger/smaller $[\text{Fe}/\text{H}]$ provide *systematically* larger S . Unlike GJ 406 and GJ 699 we found that the match of observed and synthetic spectra was considerably better for data longward of $2.7 \mu\text{m}$. We suspected that this might be caused by the interference of CO $\Delta\nu = 2$ bands, so we investigated higher ($\log N(\text{C}) = -3.13$) and lower ($\log N(\text{C}) = -3.68$) carbon abundances than the scaled solar value ($\log N(\text{C}) = -3.48$), however, we found no evidence that the dis-

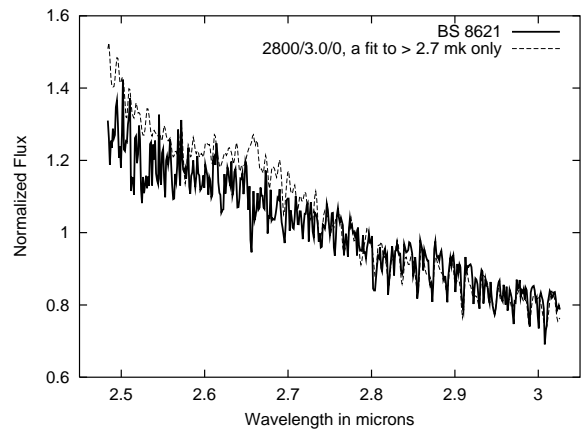


Figure 17. The observed spectrum of BS 8621 compared to a 2800 K, $\log g = 3.0$, solar metallicity synthetic spectrum.

crepancies are caused by CO. Since the incompleteness of the water line list increases with increasing temperature (e.g., Fig. 8) it is to be expected that the spectrum of GJ 191 is less well fit than the cooler dwarfs. Allard et al. (2000) reach a similar conclusion using the PS line list: ‘The introduction of the PS-H₂O opacities brings solid improvements of the near-infrared SED of late-type dwarfs but fails as the AH95 models did to reproduce adequately the J-K colors of hotter stars’. Despite these problems a reasonable match between the observed and synthetic spectra can be seen in Fig. 16.

5.6 BS 8621

BS 8621 is a giant star with a well determined spectral type of M4III. Unlike the cool dwarfs previously considered it is likely that the oxygen (and carbon) abundances in its atmosphere may be altered due to nuclear processing. Nonetheless there are no indications in the literature that this well studied object has a composition different from solar so we start with the simplifying assumption that oxygen and carbon abundances in the atmosphere of BS 8621 are solar: $\log N(\text{O}) = -3.14$ and $\log N(\text{C}) = -3.48$ (Grevesse & Anders 1989).

At a given temperature we expect that water bands

Table 2. Best fit models for the sample and a collection of effective temperatures and metallicities from the literature. The value for BS 8621 is given without an error to reflect the uncertainty in this value. References are as follows (1) Krawchuk, Dawson & De Robertis (2000), (2) Gizis (1997), (3) Leggett (1992), (4) Cayrel de Strobel et al. (1985), (5) Bessell (1991), (6) Tinney et al. (1993), (7) Jones et al. (1994), (8) Leggett et al. (2000, *apj*, 535, 965), (9) Reid & Gilmore (1984), (10) Veeder (1977), (11) Pettersen (1980), (12) Mould (1976), (13) Basri et al (2000), (14) Kirkpatrick et al. (1993), (15) Tsuji et al. (1996), (16) Berriman et al. (1992), (17) Brett (1995), (18) van Belle et al. (2000).

Object	Best fit model	Values of T_{eff} (and $[\text{Fe}/\text{H}]$) from the literature (Reference given in caption)
GJ 191	3700±100 K, [Fe/H]=−1.0±0.3	3466 −1.82(1), 3700 −1.5(2), −0.5 (4), 3550 −0.55 (12)
GJ 699	3300±100 K, [Fe/H]=−0.5±0.3	2924 −1.35 (1), 3500 −0.5 (2), 3250(5), 3110 (6), 3095(7), 3100 −0.0 (8), 3250 (9), 3110 (14), 3210 (15), 3130 (16), 3140 (17)
GJ 406	3000±100 K, [Fe/H]=−0.5±0.5	2800(5), 2580(6), 2670(7), 2600 −0.0 (8), 2850 (9), 2800 (10), 2500 (11), 2800 (13), 3000 (14), 2800 (15), 2565 (16), 2600 (17)
BS 8621	2800 K	3375–3475 (18)

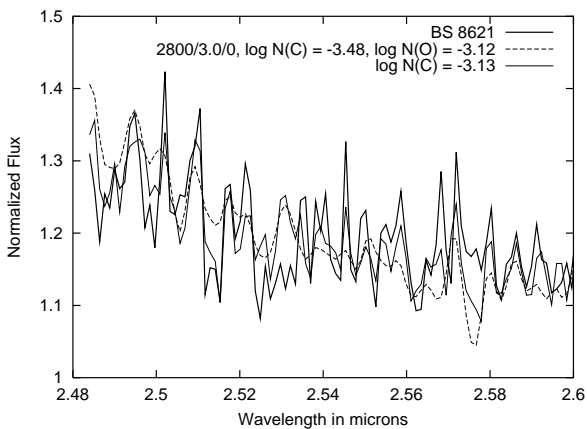


Figure 18. The observed spectrum of BS 8621 compared to 2800 K, $\log g = 3.0$ synthetic spectra with two different carbon abundances. The influence of an enhanced carbon abundance can be seen prominently on the CO bands between 2.49 and 2.52 μm .

should weaken towards lower gravities as pressure broadening lessens in importance. Although BS 8621 has a lower gravity and an early M spectral type, its spectrum has similar spectral features although a somewhat different spectral shape. As for the M dwarfs its spectrum is clearly dominated by water vapour. However, the spectrum is markedly different on the left-hand side from the right-hand side. The longer wavelength side is well fit by a 2800K $\log g = 3.0$ model, see Fig. 17. Though at wavelengths shorter than about 2.7 μm , water vapour absorption does not completely dominate the spectrum. It appears that transitions of CO $\Delta\nu=2$ maybe important. In order to explain the $< 2.7 \mu\text{m}$ spectrum with CO features it is necessary to considerably *increase* the carbon abundance. This allows the CO features to be more clearly seen against the background of water vapour features. In Fig. 18 a synthetic spectrum with a carbon abundance of $\log(C) = 3.13$ considerably improves the fit relative to a synthetic spectrum with a solar abundance pattern ($\log(C) = -3.48$, $\log N(\text{O}) = -3.12$). From the literature BS 8621 appears to be accepted as a close to solar metallicity standard M4III though Lazaro et al. (1991) find that BS 8621 has a reduced carbon abundance $[\text{C}/\text{H}]=-0.5$. Lazaro et al.’s result thus supports the expectation that the

C/O ratio in giants such as BS 8621 may be considerably modified by the CN-cycle. Such a drastic change in carbon abundance appears to have a relatively small effect on the synthetic spectra longward of 2.7 μm (Fig. 17) where CO bands are considerably weaker. In order to properly investigate this we need to use structural models computed for a variety of C/O ratios. Such models are not currently available to us and anyways are beyond the scope of the current paper where we wish to investigate the regime where water vapour is the dominant opacity, e.g. Fig. 5.

5.7 Discussion

We have investigated a variety of model fits for a range of M stars. These are particularly promising for our cooler targets. In Table 2 we present best fit parameters for our sample though it is important to note that our study of the sensitivity of the spectra to the various model parameters is arguably more lasting than our determination of T_{eff} , $\log g$, and $[\text{Fe}/\text{H}]$ values. We could have picked out these values much more quickly by eye though we preferred do this systematically and thus be able to quantify the sensitivity of the spectra to different model parameters.

In general the temperatures that we find are relatively high in comparison with the literature values which were obtained with a variety of different methods. An immediate concern is that our temperature for GJ 699 is higher than the 3100 K obtained for the benchmark eclipsing binary system CM Dra composed of two M4.5 stars (Viti et al. 1997). The bolometric luminosity for GJ 699 is lower by around 20% so it would be expected to have a lower temperature than CM Dra. However, Viti et al. (2001) have recently demonstrated that CM Dra has a lower metallicity than GJ 699 by around 0.5 dex. Based on Chabrier & Baraffe (1997) for a given luminosity this lower metallicity will cause a smaller radius by around 3% or more which may compensate for the luminosity difference allowing our temperature for GJ 699 to be just acceptable. One possibility is that the effective temperature measured by spectra from 2.5 — 3.0 μm is not a good reflection of effective temperature of the spectral energy distribution. Since the opacity of water vapour dominates the infrared opacity budget and is particularly high in this region we would expect to see little contribution at $\tau \sim 1$ in this region from deeper hotter layers thus we

would actually expect to see cooler effective temperatures than expected but not hotter. A more plausible explanation for the high temperatures we find is the non-physical line splittings of the PS line list. These are likely to over predict the strength of water vapour transitions for a given temperature. This will lead to higher temperatures being fit to a given observed spectrum.

We found very good fits for GJ 699 and GJ 406, however, our fits for GJ 191 and BS 8621 are not so impressive. We consider that the relatively poorer fit for GJ 191 arises because of its higher temperature though we attribute our fitting problems with BS 8621 to the relative importance of CO in its atmosphere. For the case of GJ 191, our fit parameters are within the wide spread of parameters found by other authors. In contrast to the relatively high temperatures found for dwarfs our formal solution for the giant finds a significantly low temperature. We observe water vapour bands that are considerably stronger than are expected for its low gravity. Given that the temperatures for M4III giants are determined using interferometry results our 600 K lower temperature are notable! However, our fit to BS 8621 does not account properly for its apparent CO absorption bands. The evidence from Lazaro et al. (1991) is that BS 8621 is carbon deficient. A lower value of $\log N(C)$ is likely to dramatically alter the chemical equilibrium, and as a result, CO and H₂O opacities and the temperature structure of the model atmosphere. In particular the CO opacity will decrease with a corresponding increase in H₂O opacity. This increase in H₂O opacity is likely to be important across a wide range of effective temperatures. In the case of BS 8621 this increase in H₂O opacity will lead to an increase in the relative strength of water bands for a given temperature and thus cause us to fit BS 8621 to a higher temperature. Furthermore, as discussed above, we expect this spectral region to yield relatively low temperatures. This idea will soon be tested as van Belle et al. (2001) are investigating the different effective temperatures found when using effective radius measurements made at different wavelengths from V to K. Another part of the solution to resolve the temperature discrepancy is likely to be provided by the presence of a warm molecular sphere residing above the photosphere, the so-called MOLsphere (Tsuji 2000a & 2000b). However, given that we do see CO bands from 2.5–2.7 μm it is not possible to properly test this scenario until spectral analysis has been done with appropriate structural models and a variety of C/O ratios.

6 CONCLUSIONS

Observations of water vapour show a good match with previous ground-based observations and indicate that the PS line list predicts the positions and intensities of water vapour well enough to use for the determination of effective temperatures. The PS line list is a substantial improvement on the MT line list which has been widely used for the generation of synthetic spectra of M dwarfs. The SCAN line list produced results substantially different from the observations and other models. The effective temperatures we determined are reasonably consistent with other methods of temperature measurement. Although the complex spectral energy distributions of cool dwarfs caused by water vapour

have traditionally hampered reliable temperature determinations, it now seems feasible that observations of water rich regions coupled with the next generation of water vapour line lists might become the method of choice for the temperature determination of cool dwarfs. Our work indicates that most sensitive best fits will be obtained when analysing high resolution data.

However, a further conclusion of this work, in agreement with that of Allard et al. (2000), is that the presently available water linelists are still not good enough to generate accurate spectroscopic models of cool stars. These linelists have however been instrumental in improving the interpretation of hot water, e.g. in sunspots (Polyansky et al. 1997b); as a result there are now significantly more experimental data available on water (Tennyson et al. 2001). These data are being used to greatly improve the effective potential energy surfaces for water which, when combined with the improved dipole surface due to Schwenke & Partridge (2000), should make an excellent starting point for generating a new linelist. Experience, such as the tests performed in this paper, show that all aspects of such calculations need to be of very high quality if a satisfactory water opacity is to be obtained.

ACKNOWLEDGMENTS

We thank Peter Hauschildt for synthetic spectra, David Schwenke for water vapour data, David Goorvitch for CO data and Iain Steele for organising the initial programme files in Nordvijk, ESA. We are also grateful to Kieron Leech and Alberto Salama for their assistance with data reduction. Takashi Tsuji and the anonymous referee are warmly thanked for their critical readings of this paper. ISO is an ESA project with instruments funded by ESA Member States (especially the PI countries: France, Germany, the Netherlands and the United Kingdom) and with the participation of ISAS and NASA. The ISAP is a joint development by the LWS and SWS Instrument Teams and Data Centers. Contributing institutes are CESR, IAS, IPAC, MPE, RAL and SRON. YPs studies are partially supported by a Small Research Grant from American Astronomical Society.

REFERENCES

- Allard F., Hauschildt P., 1999, *ApJ*, 540, 1005
- Allard F., Hauschildt P., Schwenke D.W., 2000, *ApJ*, 540, 1005
- Allen C.W., 1973, *Astrophysical quantities*, The Athlone Press, University of London.
- Anders E., Grevesse N., 1989, *Geochimica et Cosmochimica Acta*, 53, 197
- Basri G., Mohanty S., Allard F., Hauschildt P.H., Delfosse X., Martin E.L., Forveille T., Goldman B., 2000, *ApJ*, 538, 363
- Berriman G., Reid N., Leggett S.K., 1992, *ApJ*, 392, 31
- Bessell M.S., 1991, *AJ*, 101, 662
- Brett J.M., 1995, *A&A*, 295, 736
- Cayrel de Strobel G., Bentolila C., Hauck B., Duquennoy A., 1985, *A&AS*, 59, 145
- Chabrier G. & Baraffe I., 1997, *A&A*, 327, 1039
- Goorvitch, D., 1994, *ApJS*, 95, 535
- de Graauw T. et al., 1996, *SWS instrument manual*, ESA special publication
- Gizis J., 1997, *AJ*, 113, 806

- Gurtovenko E.A., Kostyk R.I., 1989, Fraunhofer spectrum and system of solar oscillator strengths, Kiev, Izdatel'stvo Naukova dumka, 200
- Hauschildt P.H., Allard F., Baron E., 1999, *ApJ*, 512, 377 <http://dilbert.physast.uga.edu/~yeti/mdwarfs.html>
- Heras, A.M., Shipman, R.F., Price, S.D., de Graauw, Th., Waters, L.B.F.M., Walker, H.J., de Muizon, M. Jourdain, Kessler, M.F., Prusti, T., 1997, *Astrophysics and Space Science*, 255, 251
- Jones H.R.A., Longmore A.J., Jameson R.F., Mountain C.M., 1994, *MNRAS*, 267, 413
- Jones H.R.A., Longmore A.J., Hauschildt P., Allard F.A., Miller S., Tennyson J., 1995, *MNRAS*, 277, 767
- Jones H.R.A., Longmore A.J., Hauschildt P., Allard F.A., 1996, *MNRAS*, 280, 77
- Jones H.R.A., Viti S., Miller S., Tennyson J., Hauschildt P., 1996, 9th Cambridge workshop on cool stars, stellar systems and the Sun, ASP, 109, 717, ed. Pallavicini, R., Dupree, A.K., Astronomical Society of the Pacific, San Francisco
- Jorgensen U.G., Jensen P., Sorensen G.O., Aringer B., 2001, *A&A*, 372, 249
- Kirkpatrick J.D., Kelly D.M., Rieke G.H., Liebert J., Allard F., Wehrse R., 1993, *ApJ*, 402, 643
- Krawchuk C.A.P., Dawson P.C., De Robertis M.M., 2000, *AJ*, 119, 1956
- Kupka, F., Piskunov, N., Ryabchikova, T. A., Stempels, H. C., Weiss, W. W., *A&AS*, 1999, 138, 119
- Lazaro C., Lynas-Gray A.E., Clegg R.E.S., Mountain C.M., Zadrozny A., 1991, *MNRAS*, 249, 62
- Leggett S.K., 1992, *ApJS*, 82, 351
- Leggett S.K., Allard F., Dahn C., Hauschildt P.H., Kerr T.H., Rayner J., 2000, *ApJ*, 535, 965
- Lutz D., Feuchtgruber H., Morfill J., 2000, MPE-ISO-99-1
- Lynas-Gray A.E., Miller S., Tennyson J., 1995, *J. Mol. Spectrosc.*, 169, 458
- Miller S., Tennyson J., Jones H.R.A., Longmore A.J., 1994, in *Proc. IAU Colloq.* 146, Jorgensen U.G., Thejl Pl, eds, Springer-Verlag, Berlin, p. 296
- Mould J.R., 1976, *ApJ*, 210, 402
- Partridge H., Schwenke D.W., 1997, *J.Chem. Phys.*, 106, 4618
- Pavlenko Y., 2000, *Ast. Rep.*, 44, 219
- Pavlenko, Y. 2001, *Ast. Rep.*, 45, 144
- Petterson B.R., 1980, *A&A*, 82, 53
- Polansky O.L., Tennyson J., Viti S., Bernath P.F., Wallace L., 1997a, *ApJ*, 489, L205
- Polansky O.L., Zobov N.F., Tennyson J., Viti S., Bernath P.F., Wallace L., 1997b, *Journal Molecular Spectroscopy*, 186, 422
- Reid I.N., Gilmore G., 1984, *MNRAS*, 206, 19
- Rothman L.S., Rinsland C.P., Goldman A., Massie S.T., Edwards D.P., Flaud J.-M., Perrin A., Camy-Peyret C., Dana B., Mandin J.-Y., Schroeder J., McCann A., Gamache R.R., Wattson R.B., Yoshino K., Chance K.V., Jucks K.W., Brown L.R., Nemtchinov V., Varanasi P., 1998, *JQRST*, 60, 1
- Salama A. et al. 2000, ESA SP-419
- Schryber J.H., Miller S., Tennyson J., 1994, *JSQRT*, 53, 373
- Schwenke D.W., Partridge H., 2000, *Journal of Chemical Physics*, 113, 6592
- Tennyson J., Zobov N.F., Williamson R., Polyansky O.L., Bernath P.F., 2001, *J. Phys. Chem. Ref. Data*, in press
- Tinney C.G., Mould J.R., Reid I.N., 1993, *AJ*, 105, 1045
- Tsuji T., Ohnaka K., Aoki W., 1996, *A&A*, 305, L1
- Tsuji T., 2000, *ApJ*, 538, 801
- Tsuji T., 2000, *ApJ*, 540, 99
- Unsold, A. *Physics der Sternatmosphären*, 1955, Springer
- Valentijn E.A., Feuchtgruber H., Kester D.J.M., 1996, *A&A*, 315, L60
- van Belle G.T., Thompson R.R., PTI Collaboration, 2000, *AAS*, 197, 4502
- van den Ancker M.E., Voors R., Leech K., 1997, SWS internal report, 1.7.1997
- Veeder G., 1974, *AJ*, 79, 1056
- Viti S., 1997, PhD thesis, University of London
- Viti S., Tennyson J., Polyansky O.L., 1997, *MNRAS*, 287, 79
- Viti S., Jones H.R.A., et al., 1997, *MNRAS*, 287, 79
- Viti S., Jones H.R.A., 1999, *A&A*, 351, 1028
- Viti S., Jones H.R.A., Maxted P.F.L., Tennyson J., 2001, *MNRAS*, submitted
- Zuckerman B., Dyck H.M., 1986, *ApJ*, 311, 345

This paper has been produced using the Royal Astronomical Society/Blackwell Science \LaTeX style file.